Supplemental Information

Downregulation of the Glial GLT1 Glutamate

Transporter and Purkinje Cell Dysfunction

in a Mouse Model of Myotonic Dystrophy

Géraldine Sicot, Laurent Servais, Diana M. Dinca, Axelle Leroy, Cynthia Prigogine, Fadia Medja, Sandra O. Braz, Aline Huguet-Lachon, Cerina Chhuon, Annie Nicole, Noëmy Gueriba, Ruan Oliveira, Bernard Dan, Denis Furling, Maurice S. Swanson, Ida Chiara Guerrera, Guy Cheron, Geneviève Gourdon, and Mário Gomes-Pereira

SUPPLEMENTAL TABLES

Table S1. Clinical data of control individuals (related to Figure 4).

	Non-DM controls			
	a	**b**	**c**	**d**
Sex	M	M	M	M
Diagnosis	N/A,	Charcot-Marie-Tooth Disease;	Rheumathoide arthritis	Limb-girdle muscular dystrophy
Neuropsychological profile	N/D	N/D	N/D	N/D
Neuroimaging	N/D	N/D	N/D	N/D
Age; cause of death	79; *Pneumocystis* pneumonia	71; pneumonia	76; interstitial pneumonia	66; cardiac failure

Table S2. Clinical data of DM1 individuals (related to Figure 4).

	DM1 samples						
	e	**f**	**g**	**h**	**i**	**j**	**k**
Sex	F	F	F	M	F	M	M
CTGs in blood (age of analysis)	1300-1400 (40)	>2500 (N/D)	N/D	N/D	1730 (73)	700-1100 (30)	1600-1800 (40)
CTGs in cerebellum (age of analysis)	400 (69)	450 (64)	200 (62)	500 (58)	350 (73)	350 (67)	400 (62)
Age of onset	40	Unknown	54	46	40	30	40
Clinical form of DM	Adult DM1	N/D	Late onset DM1	Adult DM1	Adult DM1	Adult DM1	Adult DM1
DM main symptoms	Gait problems	Gait problems	Cardiac arrhythmia; gait problems	Limb muscle weakness	Muscle weakness and atrophy in all extremities	Gait problems	Gait problems
Neuropsychological profile	WAIS-R (VIQ74, PIQ73, IQ73)	N/D	N/D	N/D	Memory loss	N/D	N/D
Neuroimaging	Diffuse atrophy	General brain atrophy	N/D	N/D	Bilateral fronto-temporal atrophy	N/D	Normal
Age; cause of death	69; pneumonia	64; ARDS	62; pneumonia	58; pneumonia	73; pneumonia	67; pneumonia	62; heart failure

ARDS, acute respiratory distress syndrome; N/A not applicable; N/D, not determined.

Table S3. Primary antibodies for immunofluorescence and immunohistochemistry (related to Figures 1 and 4).

Antigene	Supplier; vendor reference; RRID	Species origin	Blocking and incubation conditions	Ab dilution
CALB1	Swant; CB38; AB_10000340	mouse	10% NGS, 1h, RT	1/400
FOX1	Abcam; ab83574; AB_1859807	mouse	10% NGS, 1h, RT	1/400
FOX2	Abcam; ab57154; AB_2285090	mouse	10% NGS, 1h, RT	1/400
GFAP	DakoCytomation; Z0334; AB_10013382	rabbit	10% NGS, 1h, RT	1/400
GLAST	Abcam; ab416; AB_304334	rabbit	10% NGS, 1h, RT	1/200
GLT1	Alomone; AGC-022; AB_2039891	rabbit	10% NGS, 1h, RT	1/200
MBNL1	MB1A from Glen Morris (gift)	mouse	0.1% BSA, 10% NGS, 1H, RT	1/10
MBNL2	MB2A from Glen Morris (gift)	mouse	0.1% BSA, 10% NGS, 1h, RT	1/10
NeuN	Chemicon; MAB377; AB_2298772	mouse	10% NGS, 1h, RT	1/400
Ubiquitin	Dako Cytomation; Z0458; AB_2315524	rabbit	10% NSS, 1h, RT	1/500

BSA, bovine serum albumin; NGS, normal-goat serum; NSS, normal swine serum; RT, room temperature.

Table S4. Oligonucleotide primers sequences for RT-PCR analysis of laser micro-dissected mouse cells (related to Figure 1).

Gene	Exon	Primer 1	Primer 2	Primer 3	PCR product size (bp)
Calb1	N/A	GTGCTTTGGGTGACAGTCCT	TGAGCTGGATGCTTTGCTGA	TGGATTTCCCCGAAAATCTACCA	139
Glast	N/A	GGGGAGCACAAATCTGGTGA	CCGTGCCTGGATCTGTGAAT	GTAACCCGGAAGAACCCCTG	159
Mbnl1	7	CAATGTTGGTCACGGGGAATC	GCTGCCCAATACCAGGTCAAC	TGGTGGGAGAAATGCTGTATGC	270/216
Mbnl2	5	CCATAGGGACAAATGCGG	ACCGTAACCGTTTGTATGGATTAC	TTGGTAAGGGATGAAGAGC	255/201

N/A, not applicable.

Table S5. Oligonucleotide primer sequences for mouse and human RT-PCR analysis (related to Figure 1).

Gene	Species	Exon	Forward primer	Reverse primer	PCR product size (bp)
18S	Mouse	qRT-PCR	CAGTGAAACTGCGAATGG	CGGGTTGGTTTTGATCTG	165
18S	Human	qRT-PCR	CAGTGAAACTGCGAATGG	CGGGTTGGTTTTGATCTG	165
Fabp7	Mouse	qRT-PCR	TACATGAAAGCTCTGGGCGTG	TGTCCGGATCACCACTTTGC	105
Glt1	Mouse	Whole transcript	CCGTTAAATACCGCTCTCCGC	GCTGGGGAGTTTATTCAAGAATTG	1854
Glt1	Mouse	13	TGCTGGAACTTTGCCTGTTACC	GTGTTGGGAGTCAATGGTGTCC	433/298
Glt1	Mouse	Intron 11	TCATCGCCATCAAGGACTTAGAAG	GCTGGGAATACTGGCTGC GAGAGAAACAGGAAGCAGCAAATG	-In11: 434 +In 11: 266
Glt1	Mouse	qRT-PCR	TGGACTGGCTGCTGGATAGA	CGGTGTTGGGAGTCAATGGT	118
GLT1	Human	Whole transcript	ACCGTCCTCTGCCACCACTCT	ACGCTGGGGAGTTTATTCAAGAAT	2194
GLT1	Human	12	TTTGCCTGTCACCTTTCGTTG	TTAGAGTTGCTTTCCCTGTGGTTC	504/369
GLT1	Human	Intron 10	GGCAACTGGGGATGTACA	ACGCTGGGGAGTTTATTCAAGAAT CCAGAAGGCTCAGAAGT	-In10: 835 +In10: 345
GLT1	Human	qRT-PCR	TAGCCGCCATCTTTATAGCCC	CGGCTGTCAGAATGAGGAGC	150
MAPT/ TAU	Human	10	CTGAAGCACCAGCCAGGAGG	TGGTCTGTCTTGGCTTTGGC	367/274
Mbnl1	Mouse	7	TGGTGGGAGAAATGCTGTATGC	GCTGCCCAATACCAGGTCAAC	270/216
MBNL1	Human	7	TGGTGGGAGAAATGCTGTATGC	GCTGCCCAATACCAGGTCAAC	270/216
Mbnl2	Mouse	5	CTTTGGTAAGGGATGAAGAGCAC	ACCGTAACCGTTTGTATGGATTAC	255/201
MBNL2	Human	5	CTTTGGTAAGGGATGAAGAGCAC	ACCGTAACCGTTTGTATGGATTAC	255/201
Sept4	Mouse	qRT-PCR	GGTGGCAGGAGAATCTGGTC	CCGATCCCGGTACAAGTCAG	76
β-ACTIN	Human	N/A	CCGTCTTCCCCTCCATCG	CCTCGTCGCCCACATAGG	87
Tbp1	Mouse	N/A	GGTGTGCACAGGAGCCAAGAGTG	AGCTACTGAACTGCTGGTGGGTC	192
TBP1	Human	N/A	GGTGTGCACAGGAGCCAAGAGTG	AGCTACTGAACTGCTGGTGGGTC	192

qRT-PCR, quantitative RT-PCR; -In10, intron 10 exclusion; +in10, intron 10 inclusion; -In11, intron 11 exclusion; +in11, intron 11 inclusion; N/A, not applicable.

Table S6. Primary antibodies for western blot immunodetection (related to Figure 3, 4, 5 and 6).

Antigene	Supplier; vendor reference; RRID	PAGE (%)	Species origin	Blocking and incubation conditions	Ab dilution
Actin	BD Biosciences; 612656; AB_2289199	10-12	mouse	5% blotto, 1h, RT	1/5,000
CALB1	Swant; cb38; AB_10000340	12	rabbit	5% blotto, 1h, RT	1/500,000
CALB2	Abcam; ab1550; AB_90764	12	rabbit	5% blotto, 1h, RT	1/5,000
CELF1	Millipore; 05-621; AB_309851	10	mouse	5% blotto, 1h, RT	1/1,000
CELF2	Sigma; C9367; AB_1078584	10	mouse	5% blotto, 2h, RT	1/1,000
GAPDH	Genetex; GTX627408; AB_11174761	10-12	mouse	5% blotto, 1h, RT	1/10,000
GLAST	Abcam; ab416; AB_304334	10	rabbit	5% blotto, 1h, RT	1/5,000
GLT1	Alomone; AGC-022; AB_2039891	10	rabbit	5% blotto, 1h, RT	1/1,000
GLUR2	Abcam; ab206293; N/A	10	rabbit	5% blotto, 1h, RT	1/2000
NMDAR1	ThermoFisher Scientific; 32-0500; AB_2533060	10	mouse	5% blotto, 1h, RT	1/500
PSD95	Abcam; ab2723; AB_303248	10	mouse	5% blotto, 1h, RT	1/1000
PVALB	Millipore; MAB1572; AB_2174013	12	mouse	2.5 BSA, 1h, RT	1/500

N/A, not applicable; RT, room temperature.

Table S7. Sequences of MBNL1 and MBNL2 shRNA (related to Figure 5).

Gene	Sequence	Complementary sequence
MBNL1	AACACGGAAUGUAAAUUUGCA TT	UGCAAAUUUACAUUCCGUGUUTT
MBNL2	CACCGUAACCGUUUGUAUTT	CAUACAAACGGUUACGGUTT

SUPPLEMENTAL FIGURES
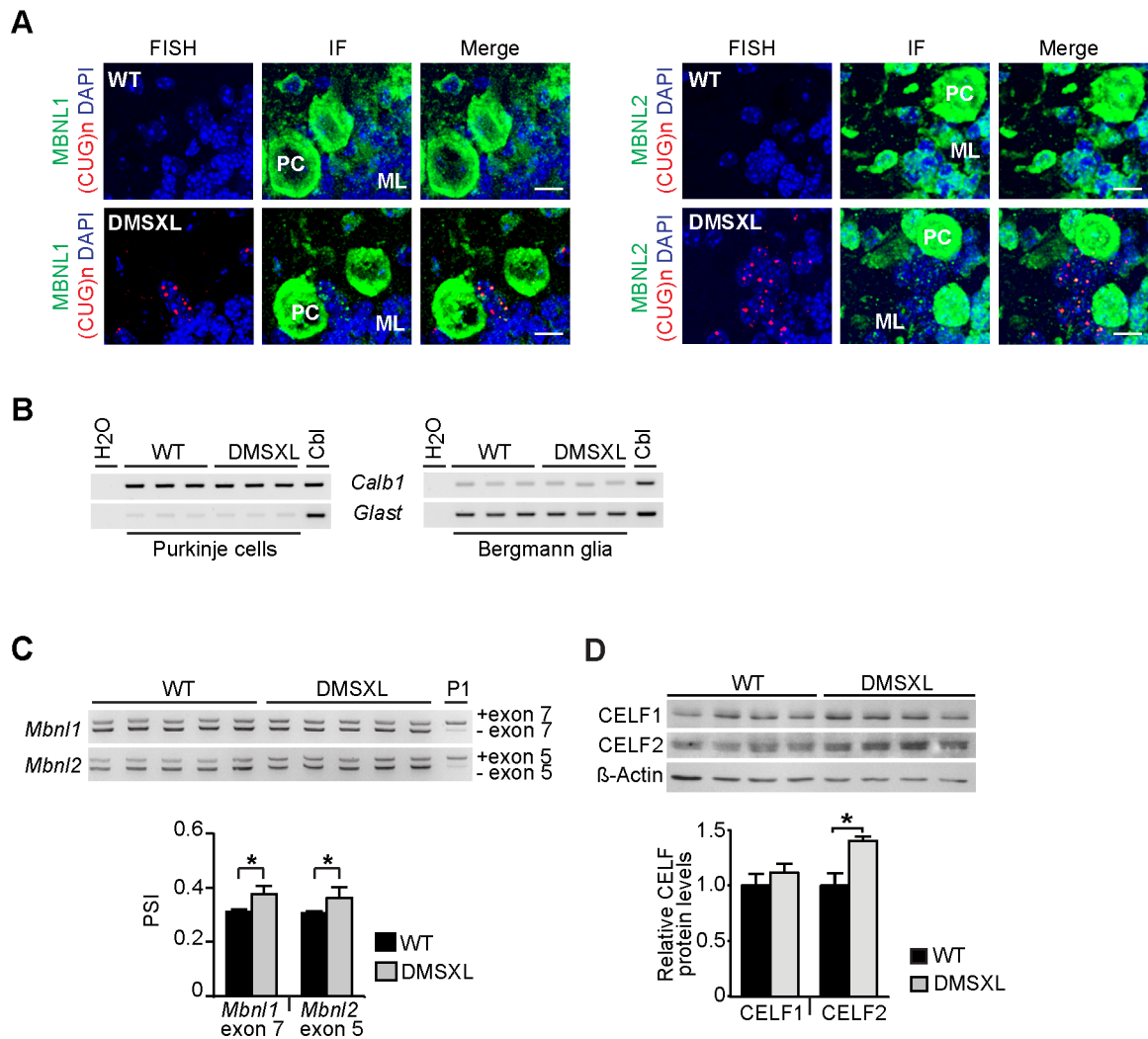
Figure S1. RNA foci, splicing and CELF protein levels in DMSXL cerebellum (related to Figure 1). (A) FISH detection of RNA foci (red) and immunofluorescence of MBNL1 and MBNL2 (green) in WT and DMSXL mouse cerebellum. The scale bar represents 10 µm. PC, Purkinje cells; ML, molecular layer. **(B)** RT-PCR expression analysis of RNA transcripts primarily expressed in Purkinje cells (calbindin 1, *Calb1*) and in Bergmann glia (*Glast*), to confirm the nature of the cells collected by laser cell microdissection from the cerebellum of WT and DMSXL mice (n=3 animals, each genotype). *Calb1* transcripts were found predominantly in collected Purkinje cells, while *Glast* showed higher expression in microdissected Bergmann astrocytes. H_2O, no DNA control; Cbl, mouse cerebellum tissue control. **(C)** RT-PCR analysis of splicing profiles of *Mbnl1* and *Mbnl2* mRNA transcripts in the cerebellum of 2-month-old DMSXL and WT mice (n=5, each genotype) and in WT newborn animals (P1, pool of 3 animals). The graphs represent the mean PSI (±SEM) of alternative exons. **(D)** To determine the contribution of CELF protein dysregulation to missplicing, we quantified CELF1 and CELF2 levels in whole cerebellum by western blot (n=4, each genotype). The graphs represent the mean (±SEM) relative to normalized WT controls. Only CELF2 was significantly upregulated in DMSXL mice. ß-Actin was used as internal control. *$P<0.05$; Mann-Whitney U test.
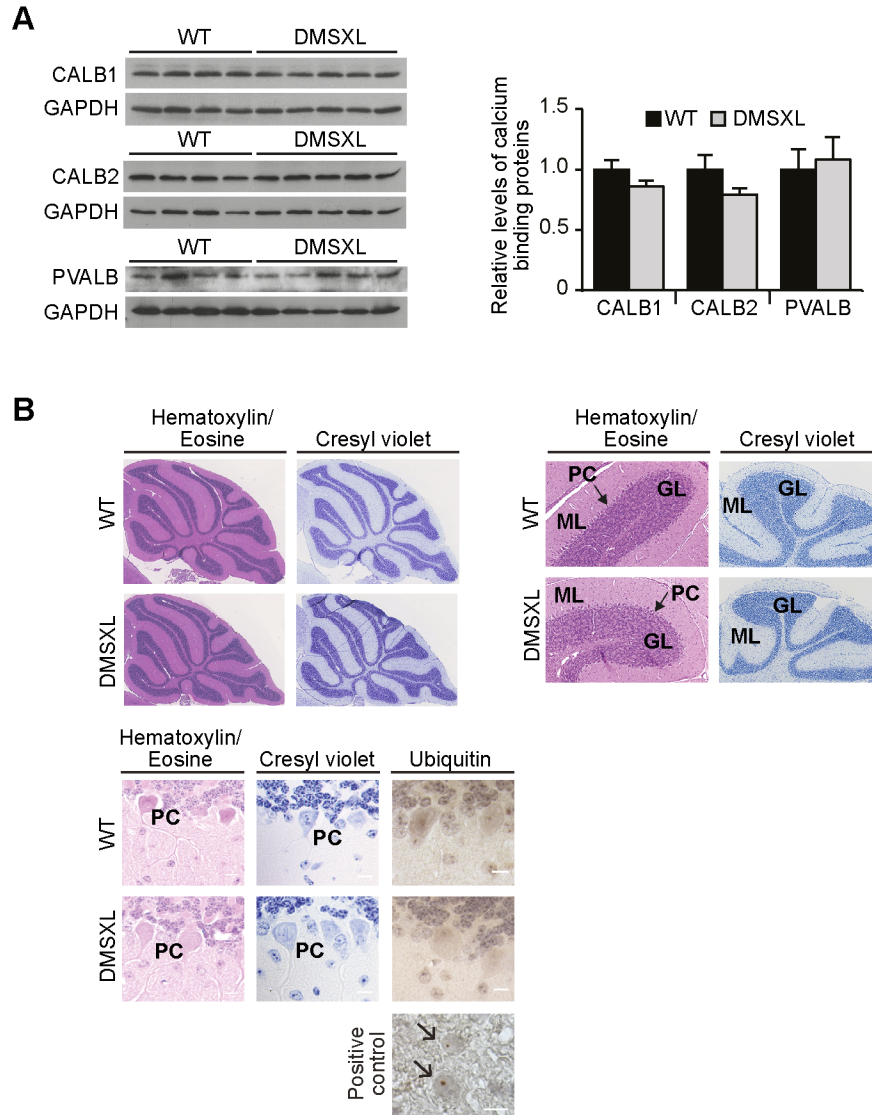
Figure S2. Expression of calcium-binding proteins is not altered in DMSXL cerebellum (related to Figure 2). (A) Western blot analysis of key calcium-buffering proteins (calbindin 1, CALB1; calbindin 2/calretinin, CALB2; and parvalbumin, PVALB) in the cerebellum of DMSXL mice (n=5), relative to WT controls (n=4). The graphs represent average protein levels (±SEM), relative to normalized WT controls. GAPDH was used as loading control. No significant difference was found in protein levels in DMSXL cerebellum. **(B)** Signs of neurodegeneration and histopathology in DMSXL cerebellum were investigated by standard hematoxylin-eosin and cresyl violet staining. Proteotoxicity was studied by the immunodetection of ubiquitin aggregates. Lower magnification pictures (top panels) do not show evidence of overall changes in cerebellum structure, morphology or cell density in DMSXL mice. Higher magnification pictures (bottom panels) do not reveal obvious changes in cell morphology, neurodegeneration or ongoing protein stress. FXTAS knock-in mouse brains were used as positive controls for the accumulation of ubiquitin-containing protein aggregates. PC, Purkinje cell; GL, granular layer; ML, molecular layer.
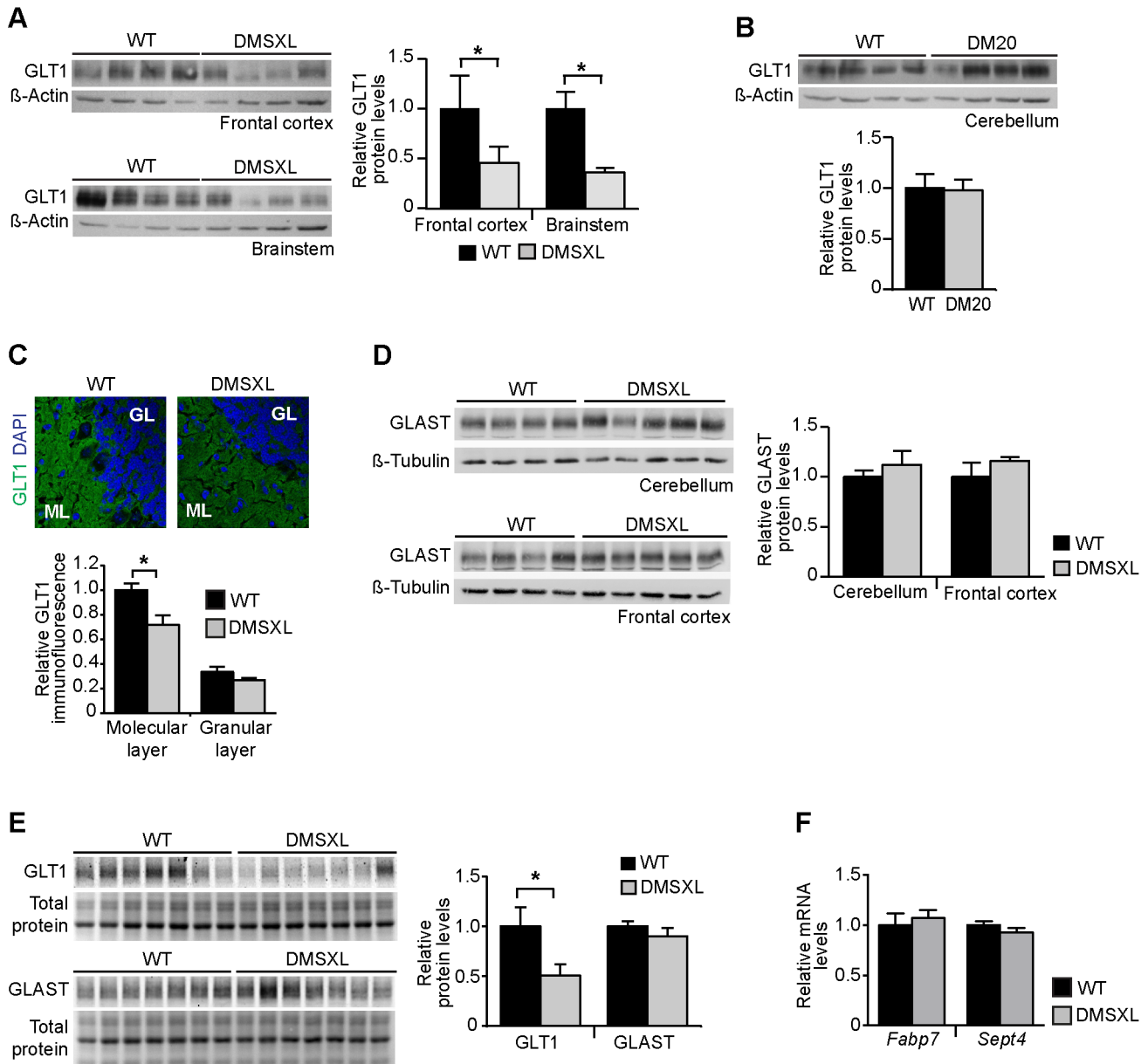
Figure S3. **GLT1 is downregulated in multiple brain regions of DMSXL mice (related to Figure 3). (A)** To assess the extent of GLT1 downregulation, we quantified GLT1 protein levels in additional brain regions from 2-month-old mice by western blot. GLT1 protein was significantly downregulated in the frontal cortex and brainstem of DMSXL mice, compared to WT controls (n=4, each genotype). ß-Actin was used as loading control. **(B)** Quantification of GLT1 protein levels in control DM20 transgenic mice, relative to WT littermates (n=4, each genotype). Overexpression of short *DMPK* transcripts is not sufficient to affect GLT1 steady-state levels. **(C)** Semi-quantitative analysis of GLT1 immunofluorescence (±SEM) in the molecular and granular layers in the cerebellum of two-month-old DMSXL and WT mice. Representative pictures of three independent analyses. The same camera acquisition settings were used for both images. **(D)** Western blot analysis of GLAST protein expression in the cerebellum and frontal cortex of DMSXL (n=5) and WT mice (n=4). ß-Tubulin was used as loading control. **(E)** Quantification of GLT1 and GLAST protein steady-state levels in DMSXL and WT primary astrocytes (n=7, each genotype). Representative western blot analysis of three technical replicates. Total protein was visualized by stain-free protocols and used as loading control. GLT1 show a significant 50% reduction in DMSXL primary astrocytes, while GLAST protein levels remain unchanged. **(F)** Quantification of Bergmann-specific *Fabp7* and *Sept4* transcripts in the cerebellum of DMSXL and WT mice (n=6, each group). Graphs represent the mean ± SEM. *$P<0.05$, Mann-Whitney U test.
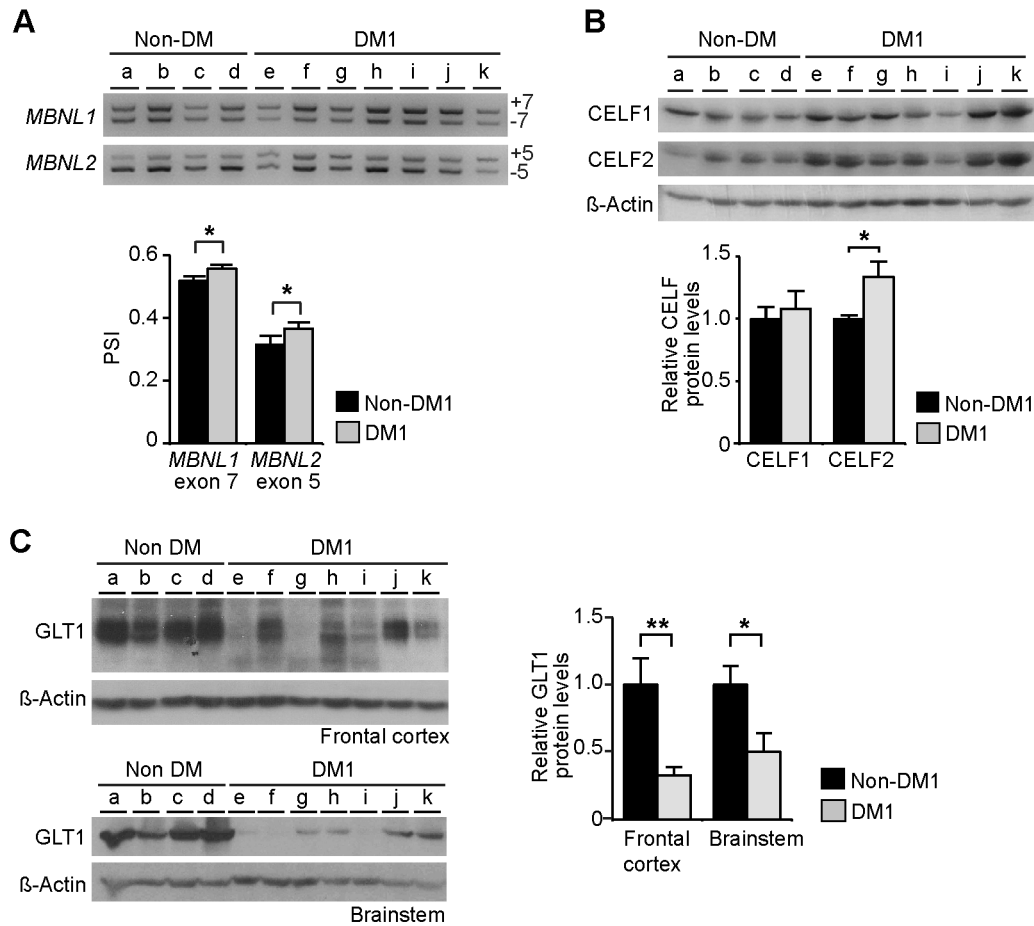
Figure S4. RNA splicing and GLT1 protein levels in human DM1 brains (related to Figure 4). (A) RT-PCR analysis of *MBNL1* exon 7 and *MBNL1* exon 5 in human cerebellum tissue samples in adult DM1 patients (n=7), relative to non-DM controls (n=4). The graphs represent the mean PSI (±SEM) of the alternative exons studied. **(B)** Quantification of CELF1 and CELF2 proteins by western blot in the cerebellum of DM1 patients (n=7), relative to non-DM controls (n=4), revealed significant upregulation of CELF2, to an extent similar to DMSXL mice. ß-Actin was used as loading control. **(C)** Western blot analysis of GLT1 steady-state levels in the frontal cortex and brainstem of adult DM1 patients and non-DM controls. GLT1 is significantly downregulated in DM1 frontal cortex and brainstem. ß-Actin was used as loading control *$P<0.05$, **$P<0.01$; Mann-Whitney U test.
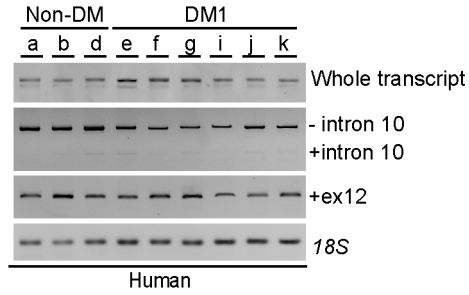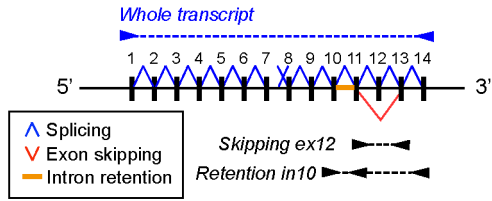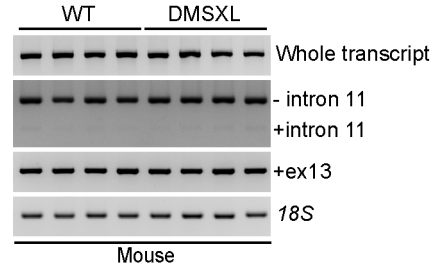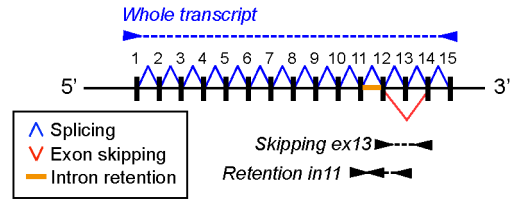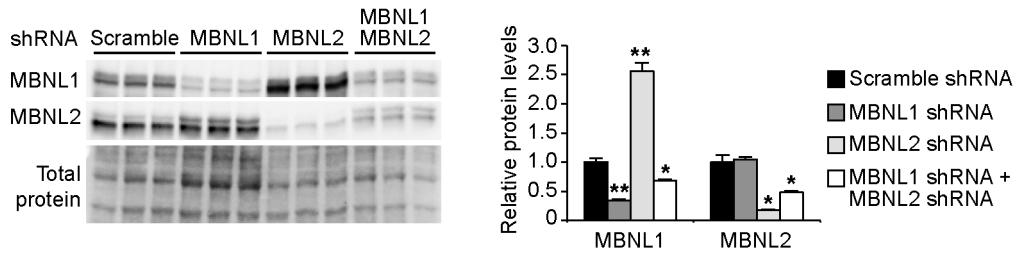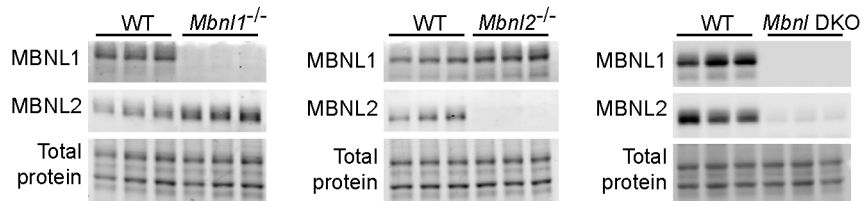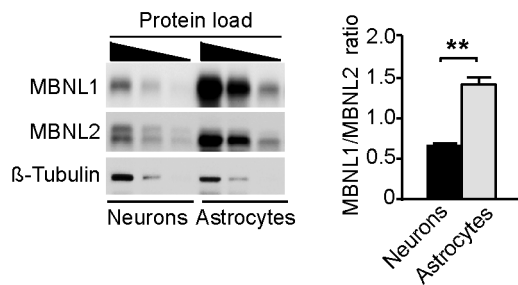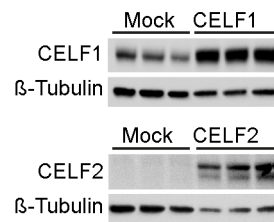
Figure S5. GLT1 downregulation is not associated with splicing abnormalities and is mediated by MBNL1 inactivation (related to Figure 5). (A) RT-PCR analysis of full-length *GLT1* mRNA, alternative exons and intron inclusion in human brains. The top illustration represents the human *GLT1* gene with 14 exons and shows the alternative splicing events studied. The arrowheads represent the location of the oligonucleotide primers used in the splicing analysis of whole transcript, skipping of exon 12 and inclusion intron 10. The results revealed no obvious differences between DM1 (n=6) and non-DM cerebella (n=3). **(B)** RT-PCR analysis of full-length *Glt1* mRNA, alternative exon 13 and intron 11 inclusion in the cerebellum of 2-month-old mice. The location of oligonucleotide primers (arrowheads) is indicated on the mouse gene. DMSXL cerebellum did not show obvious missplicing events, compared to WT controls (n=4, each genotype). **(C)** MBNL1 and MBNL2 detection by western blot following knocking down of these proteins by shRNA in T98G cells. Total protein was visualized by stain-free protocols and used as loading control. The graphs represent average protein levels (±SEM) relative to normalized scramble shRNA controls. MBNL1 was decreased down to 34% in cells transfected with MBNL1 shRNA. MBNL2 shRNA-treated cells showed MBNL2 protein levels down to 18% of scramble controls, but a 155% compensatory increase of MBNL1. MBNL1 and MBNL2 double knocking-down was more modest that individual strategies, resulting in protein levels that were 69% and 48% of those in scramble controls, respectively. **(D)** Western blot expression analysis of MBNL1 and MBNL2 proteins *Mbnl1*$^{-/-}$, *Mbnl2*$^{-/-}$ and *Mbnl* double knock out (DKO) mice, and in WT littermate controls (n=3, each genotype). Mice were aged 3-4 months. Total protein was visualized by stain-free protocols and used as loading control. **(E)** Western blot detection and quantification of MBNL1 and MBNL2 protein levels in primary neurons and astrocytes. Decreasing amounts of a protein pool of whole cell lysate from three WT cultures were electrophoresed and immunodetected. Both MBNL1 and MBNL2 proteins are more abundant in astrocytes. The graph represents the MBNL1/MBNL2 expression ratio in each cell type (mean ± SEM), and shows that MBNL1 relative expression is twofold higher in mouse primary astrocytes than in neurons. ß-Tubulin was used as loading control. **(F)** Western blot immunoblotting showing CELF1 and CELF2 upregulation in T98G cells transfected with expressing vectors. ß–Tubulin was used as loading control. *$P<0.05$, **$P<0.01$; one-way ANOVA in (C) and Mann-Whitney U test in (E).
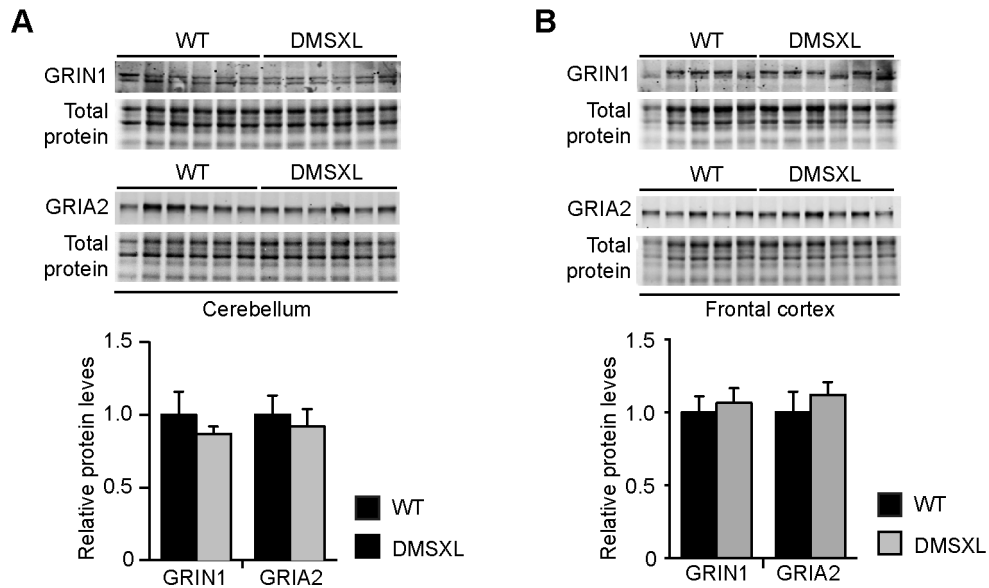
Figure S6. Glutamate receptor expression in mouse brain tissue (related to Figure 6). Quantification of GRIN1 and GRIA2 glutamate receptor subunits in the **(A)** cerebellum and **(B)** frontal cortex of 2-month-old DMSXL and WT controls (n=5-6, each genotype). Representative western blots of three technical replicates. Total protein was visualized by stain-free protocols and used as loading control. The graphs represent the mean (±SEM) relative protein levels, normalized to WT controls, and show no significant differences in the expression of glutamate receptors in DMSXL brain tissue.
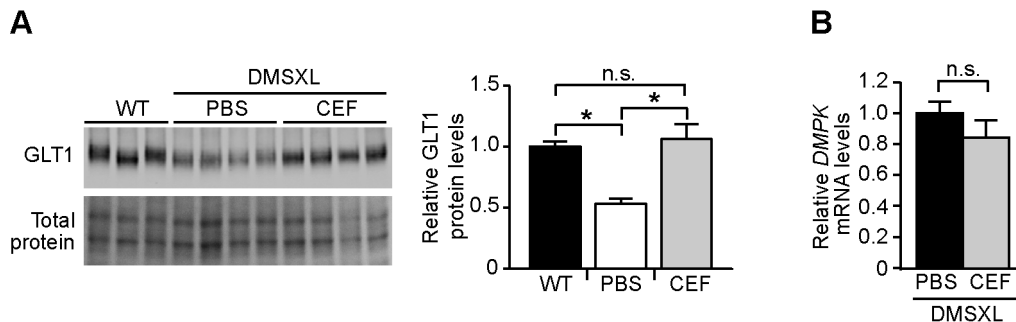
Figure S7. Ceftriaxone upregulates GLT1 but does not change *DMPK* transcript levels in DMSXL mice (related to Figure 7). (A) We confirmed that ceftriaxone increased GLT1 in DMSXL mice to levels undistinguishable from those detected in WT controls. Representative western blot analysis of GLT1 levels in the cerebellum of 2-month-old DMSXL mice following PBS or ceftriaxone treatment (200 mg/kg, daily i.p. injections, over 5 consecutive days) (n=4, each treatment group). WT controls are also shown (n=3). Total protein was visualized by stain-free protocols and used as loading control. The graph represents the mean levels of GLT1 protein (±SEM) in the cerebellum of DMSXL mice injected with ceftriaxone, PBS and in WT controls. **(B)** Real-time PCR quantification of expanded *DMPK* transcripts in the cerebellum of DMSXL mice treated with ceftriaxone (n=6) or PBS (n=6) showed no effect of the antibiotic on transgene expression. *$P<0.05$, one-way ANOVA in (A); n.s. not statistically significant, Mann-Whitney U test in (B).

SUPPLEMENTAL EXPERIMENTAL PROCEDURES AND METHODS

Mouse genotyping.
Mouse experiments were performed with wild-type controls of the same litter to reduce inter-individual variability. DMSXL transgenic mice were generated and genotyped as previously described (Gomes-Pereira et al., 2007; Hernandez-Hernandez et al., 2013). All DMSXL mice used for this work were adult (2-4 months) homozygotes, unless stated otherwise. The control DM20 line expresses non-pathogenic 20-CTG tracts (Seznec et al., 2001; Seznec et al., 2000). *Glt1* knock-out mice on C57BL/6 background (Tanaka et al., 1997) were provided by Prof. Niels Christian Danbolt (University of Oslo, Norway). The *Glt1* transgenic status was determined by multiplex PCR of tail DNA, using P1-GLT1 (5'-GGGTTGTAGATGTGTAGAGATGG-3'), P2-GLT1 (5'-CCTGACAGAGATCAGAGCACGT-3') and P3-GLT1 (5'-ATTCGCAGCGCATCGCCTTCTA-3') oligonucleotide primers. *Glt1* wild-type alleles generate a 469-bp product, while the disrupted allele generates a 210-bp allele.

Fluorescent in situ hybridization (FISH).
Ribonuclear inclusions were detected with a 5'-Cy3-labelled (CAG)5 PNA probe, as previously described (Huguet et al., 2012). Immunofluorescence (IF) combined with fluorescent *in situ* hybridization (FISH) was performed as previously described (Hernandez-Hernandez et al., 2013). Antibody references and working dilutions are listed in **Table S3**.

Laser Capture Microdissection (LCM).
Purkinje cells and surrounding cells were individually microdissected from one to two-month-old DMSXL and wild-type control mouse cerebellum, using a Palm Micro Beam (Carl Zeiss). RNA extraction, cDNA synthesis and RT-PCR analysis of candidate genes performed as previously described (Peixoto et al., 2004). Average of 100 Purkinje cells and 300 surrounding cells were separately collected in triplicate from three DMSXL mice and from three wild-type control mice. For each cDNA sample, three replicates of the RT-PCR reactions were performed. The sequences of the oligonucleotide primers used in the RT-PCR analysis of Purkinje and Bergmann cells laser microdissected from DMSXL cerebellum are listed in **Table S4**.

RT-PCR analysis of alternative splicing.
Total RNA was extracted from half mouse cerebellum collected 2-month-old mice, following tissue homogenization with stainless steel beads, and using a TRIZOL extraction protocol combined with a commercially available RNA Purification Kit, as previously described (Huguet et al., 2012). cDNA synthesis, semi-quantitative RT-PCR analysis of alternative splicing and qRT-PCR quantification of *DMPK* transcripts were performed as described elsewhere (Gomes-Pereira et al., 2007; Hernandez-Hernandez et al., 2013), using oligonucleotide primers listed in **Tables S5**. All samples were normalized to TATA-binding protein (Tbp) or ß-actin. The Percent of Spliced In (PSI) was used to quantify the splicing level of alternative exons: PSI = (intensity of inclusion isoform) / (intensity of inclusion isoform + intensity of exclusion isoform) x 100.

Western blot analysis.
Total protein was extracted from 20-30 mg brain tissue dissected from 2-month-old mice, using RIPA buffer (ThermoFisher Scientific; 89901), supplemented with 0.05% CHAPS (Sigma; C3023), 1x complete protease inhibitors (Roche; 04693124001), 1x Phospho STOP phosphatase inhibitors (Roche; 04693124001). Protein concentrations in the supernatants were determined using a Bio-Rad DCTM protein assay (Bio-Rad; 500-0114). Protein integrity was checked by Coomassie stain of a 10% SDS-polyacrylamide gel. Volumes corresponding to 30-60 µg of protein were mixed with Laemmli sample buffer and boiled for 5 min. Proteins were resolved in 10% or 12% SDS-polyacrylamide gels and transferred onto PVDF membranes. Following Ponceau red staining to verify the efficiency of protein transfer, membranes were blocked in 1X TBS-T (10 mM Tris-HCl, 0.15 M NaCl, 0.05% Tween 20) containing blotto (Santa Cruz Biotech; sc2325) and incubated overnight at 4°C with the corresponding primary antibody. After three washes with 1X TBS-T, membranes were incubated at room temperature during 1 h with the appropriated HRP-secondary antibody. Primary antibody references, working dilutions and blocking conditions are indicated in **Table S6**. After washing with 1X TBS-T, antibody binding was visualized by chemiluminiscence (PerkinElmer). Densitometric analysis with Quantity One® 1D Analysis Software (Bio-Rad) has been performed to quantify signal intensity. Quantitative western blot results are represented as means of steady-state levels (±SEM) in transgenic animals, relative to normalized controls. Total protein electrophoresed through thialo-containing polyacrylamide gels (Bio-Rad) was visualized under UV light.

Electrophysiological and behavioral assessment.
In vivo electrophysiological study in alert mice. Two-month old DMSXL and control mice were surgically prepared for chronic recording of neuronal activity in the cerebellum. The experimental session for extracellular recording of Purkinje cells (PCs) activity and local field potential (LFP) analysis in the cerebellar cortex was performed as previously described

(Cheron et al., 2004). The strength of the rhythmicity was quantified with a rhythm index (Cheron et al., 2004; Sugihara and Furukawa, 1995).

The runway test. Motor coordination was examined by the runway test as previously described (Servais and Cheron, 2005). In this test, 3-4 month old DMSXL (n=20) and control (n=21) mice, male and females included, ran along an elevated runway with low obstacles intended to impede progress. The runway was 100 cm long and 0.7 cm width. Obstacles being of 1 cm diameter wood rod and 0.7 cm width were placed every 10 cm along the runway. Mice were placed on one extremity of the runway and had to move along the runway to reach the other end. The number of slips of the right hind leg was counted. Each mouse underwent four consecutive trials per day during 5 consecutive days. The test was repeated following a test-free period of three weeks, over one day (four consecutive trials), to assess the learning capacity of mice.

iTraq proteomics analysis.

The analysis of mouse brain proteome by isobaric tagging for relative and absolute quantifications (iTRAQ) mass spectrometry was performed on individual DMSXL and wild-type male mice, aged 2 months (n=4 per genotype, for whole cell proteins extracts; n=2 for membrane bound protein fraction). Membrane-bound protein fractions were purified from mouse cerebellum, as previously described (Cox and Emili, 2006).

iTraq labeling. Protein iTRAQ labeling was performed according to the manufacturer's instructions (iTRAQ 4plex kit, ABSCIEX). Briefly, protein pellets (100 µg) were suspended in 20 µL of 500 mM triethylammonium bicarbonate (TEAB) and 1 µL of 2% SDS, they were then reduced with 2 µL of 50 mM tris-(2-carboxyethyl) phosphine (TCEP) for 1h at 60°C and finally alkylated with 1 µL of 200 mM methyl methanethiosulfonate (MMTS) for 10 min at room temperature. Proteins were digested with 2 µg of sequencing grade modified trypsin (Promega) for 16h at 37°C. The resulted peptides were labeled with iTRAQ reagents and quenched with Milli-Q water. The labeled samples were mixed in a 1:1:1:1 ratio and stored at -20°C.

Sample clean-up by SCX & Sep-Pak. An aliquot of the iTRAQ 4-plex-labeled peptide mixture (100 µg) was cleaned up with a cation-exchange cartridge SCX (from ICAT Reagent Kit, ABSCIEX), equilibrated with 10 mM potassium phosphate, pH 3, 25% acetonitrile. Peptides were eluted with 500 µL of 350 mM potassium chloride, 25% acetonitrile and concentrated in a centrifugal evaporator, under vacuum. The sample was reconstituted in 0.1% trifluoroacetic acid and loaded on a Sep-Pak cartridge (Waters) for desalting. After washing, the peptides were eluted in 1 mL of 70% acetonitrile- 0.1% trifluoroacetic acid and dried in a vacuum concentrator.

MS/MS Analysis. Nano-LC-MS/MS analysis was performed on an Ultimate 3,000 Rapid Separation Liquid Chromatography (RSLC) system (Dionex) coupled to LTQ-Orbitrap Velos mass spectrometer (Thermo Scientific). Dried peptides were resuspended in 0.1% (v/v) trifluoroacetic acid, 10% acetonitrile, and pre-concentrated on a 75 µm i.d. reversed-phase (RP) trapping column and separated with an aqueous-organic gradient (solution "A": 0.1% formic acid in 5% acetonitrile; solution "B": 0.085% formic acid in 80% (acetonitrile; flow rate 400 nl/min) on a 75 µm RP column (Acclaim PepMap RSLC 75 µm x 15 cm, 2 µm, 100Å, Dionex). Samples were eluted using a linear gradient from 5% to 40% solvent B in 190 min. One FTMS full scan was performed (resolution 60,000; positive polarity; centroid data; scan range 400 to 2,000 m/z) and the 10 most intense signals were subjected to MS/MS fragmentation both in the collision-induced dissociation (CID) cell and high-energy collision dissociation (HCD) cell for the same precursor ion. CID fragmentation was performed with a target value of 5000, collision energy of 35 V, Q value of 0.25 and activation time of 10 ms while HCD was done using a target value of 50,000, collision energy of 50 V and activation time of 0.1 ms. LC-MS/MS data were transferred to the Proteome Discoverer software v1.2 to create the .mgf file, which was searched against the *Mus musculus* subset (16547 sequences) of the UniprotKB/Swissprot database (release 2012_06; 536796 sequences) using the Mascot search engine (version 2.2.07; Matrix Science) for protein identification and protein quantification. Fixed modification (iTRAQ 4plex (K) and N-terminus) and variable modification (Methylthio (C), Oxidation (M)) were allowed as well as one missed cleavage. Monoisotopic peptide mass tolerance was ± 5 ppm (after linear recalibration), and fragment mass tolerance was ± 0.5 Da. Filters for protein quantification were set as follow: protein ratio type was "weighted", normalization was done with summed intensities and outliers were removed automatically. Only proteins quantified with at least 2 peptides and with the ion score higher than 25 were retained. False discovery rate was less than 2%. Differences between the DMSXL and WT proteomes were evaluated by a Mann-Whitney U test ($P<0.05$), as previously described (Jeanson et al., 2014). To determine the most deregulated proteins, the standard deviation of the protein ratios was calculated for each experiment, and the Gaussian distributions were normalized. An average threshold was calculated to determine the most upregulated proteins (last 20% on the right of the Gaussian) and the most downregulated proteins (first 20% on the left of the Gaussian).

GO enrichment analysis. Gene Ontology (GO) enrichment analysis of differently expressed proteins was performed using the functional annotation tool Database for Annotation, Visualization and Integrated Discovery (DAVID) v.6.7 (http://david.abcc.ncifcrf.go) (Huang da et al., 2009). GO enrichment analysis integrated the information of the cellular components and biological processes associated with the deregulated proteins, to provide a list biological terms organized into classes of related genes/proteins. Significant GO terms were identified at a FDR <0.05.

Fluorescence quantification of GLT1
Confocal images of WT and DMSXL slices of cerebellum stained on the same glass slide were acquired as z-stacks at the 40x magnification with a Leica TSC SP8 SMD Confocal microscope, using the same laser power and PMT values. Z projections were analyzed using Fiji software (Schindelin et al., 2012) by drawing the granular and molecular layer and measuring the integrated density of the regions of interest.

Tissue fractioning for western blot analysis
Cytosolic and membrane-bound protein were prepared by serial centrifugation of tissue homogenates collected from the cerebellum of 2-month-old mice, in isotonic sucrose solution, as previously described (Nishida et al., 2004). The enrichment for cytosolic and cell membrane proteins was confirmed by immunodetection of GAPDH and PSD95, respectively.

Glutamate uptake
Uptake of radioactive glutamate by cultured astrocytes was performed using published methods (Beaule et al., 2009) and expressed as fmol of radioactive glutamate per µg of total protein. Glutamate transporter inhibitors were added to the medium, to inhibit total glutamate transporter (50 µM TBOA; Bio-Techne, 10/1/2532), GLT1-mediated glutamate transport (200 nM WAY-213613; Santa Cruz Biotechnology, sc-203720) or GLAST-mediated glutamate transport (5 µM UCPH 101; Santa Cruz Biotechnology, sc-361391)

Fluorescent assay of glutamate neurotoxicity in neuroglial co-cultures
The co-cultures of neurons and astrocytes were established as previously described (Kaech and Banker, 2006). Briefly, the astrocytes were purified from the frontal cortex of P1 mouse embryos and cultured for two weeks in DMEM low glucose (31885-023Life Technologies, 31885-023), supplemented with 10% FBS and 0.05 mg/ml gentamycin (Life Technologies; 15710). E16.5 mouse neurons were dissociated from embryonic frontal cortex in a mixture of trypsin/DNase I and plated in Neurobasal-A medium (Life Technologies, 10888022), supplemented with 1X B27 supplement (Life Technologies, 17504044), 0.5 mM L-Glutamine (Life Technologies, 25030024), 1% antibiotic and antimycotic (Life Technologies, 15240-096) and 5% FBS. The primary neurons from the WT and DMSXL mice and were infected with NeuroLight[RM] red lentivirus (Essen BioScience, 4584), encoding the mKate2 fluorescent protein under the Synapsin-1 Promoter (MOI=3) four hours after plating in serum free neuronal medium. The next day neurons were washed with Neurobasal medium to remove the lentivirus and primary astrocytes, cultured two weeks, were plated on top of neurons. Neuronal fluorescence was monitored by live cell video-microscopy (IncuCyte Live Cell Analysis System, Essen BioScience), by acquiring phase contrast and red fluorescent images each hour, using the Neurotrack module of acquisition and measurement of neurite extension. On day 8 of the mixed cultures, 50 µM of glutamate were added to the medium and neurite collapse monitored for 12-24 hours. If used, glutamate receptor antagonists were also added on day 8, together with glutamate (10 µM CNQX, antagonist of AMPA receptors, Abcam, ab120017; 10 µM (+)-MK 801 maleate, antagonist of NMDA receptors, Abcam, ab144485). The rate of neurite collapse was expressed as mm of length change, per mm^2 of surface studied, per day. For the rescuing assays, GLT1 was upregulated 30 hours prior to the assessment of glutamate neurotoxicity, either by transfection of GLT1-GFP-expressing plasmids (provided by Dr. Nicolas Reyes, Institute Pasteur, Paris, France) or by treating co-cultures with 10 µM ceftriaxone.

Plasmid and shRNA transfection.
Cultured cells were transfected with 250 ng/mL to 1.25 µg/mL of plasmid DNA using JetPrime transfection reagent and protocol (PolyPlus, 114-75). shRNA was transfected at a final concentration of 200 nM using Lipofectamine RNAiMax reagent and protocol (Life Technologies; 13778150). shRNA sequences are shown in the **Table S7**.

Ceftriaxone treatment.
Mouse intraperitoneal injections of ceftriaxone (Sigma; C5793) in PBS (20 µg/µl) were performed through a 27G needle to a final dose of 200 mg/kg. Male and female mice were injected at 2 months of age, daily over a period of five days, prior to molecular, electrophysiological and behavioral assessment. Daily injections of ceftriaxone continued during motor assessment in the runway test. Treatment control mice were injected with PBS (n=5 per group, including male and females).

Microscope and images processing.
Images were taken with a fluorescent microscope Zeiss ApoTome 2 or with a Leica TSC SP8 SMD Confocal microscope. Images were treated with ImageJ software (Schneider et al., 2012).

Statistical analysis.
Statistical analyses were performed with Prism (GraphPad Software, Inc), SPSS (v14.0, SPSS Inc©), Statistica (v6.0, StaatSoft®) and/or Excel software. When two groups were compared, we first performed a normality test. Parametric data were compared using a two-tailed Student's t-test (with equal or unequal variance, as appropriate). Non-parametric data were compared using a two-tailed Mann-Whitney U test. For one-way ANOVA, if statistical significance was achieved, we performed post-test analysis to account for multiple comparisons. Statistical significance was set at $P<0.05$. The data are presented as mean ± standard error of the mean (±SEM).

SUPPLEMENTAL REFERENCES

Beaule, C., Swanstrom, A., Leone, M.J., and Herzog, E.D. (2009). Circadian modulation of gene expression, but not glutamate uptake, in mouse and rat cortical astrocytes. PLoS One *4*, e7476.

Cheron, G., Gall, D., Servais, L., Dan, B., Maex, R., and Schiffmann, S.N. (2004). Inactivation of calcium-binding protein genes induces 160 Hz oscillations in the cerebellar cortex of alert mice. J Neurosci *24*, 434-441.

Cox, B., and Emili, A. (2006). Tissue subcellular fractionation and protein extraction for use in mass-spectrometry-based proteomics. Nat Protoc *1*, 1872-1878.

Gomes-Pereira, M., Foiry, L., Nicole, A., Huguet, A., Junien, C., Munnich, A., and Gourdon, G. (2007). CTG trinucleotide repeat "big jumps": large expansions, small mice. PLoS Genet *3*, e52.

Hernandez-Hernandez, O., Guiraud-Dogan, C., Sicot, G., Huguet, A., Luilier, S., Steidl, E., Saenger, S., Marciniak, E., Obriot, H., Chevarin, C*., et al.* (2013). Myotonic dystrophy CTG expansion affects synaptic vesicle proteins, neurotransmission and mouse behaviour. Brain *136*, 957-970.

Huang da, W., Sherman, B.T., and Lempicki, R.A. (2009). Systematic and integrative analysis of large gene lists using DAVID bioinformatics resources. Nat Protoc *4*, 44-57.

Huguet, A., Medja, F., Nicole, A., Vignaud, A., Guiraud-Dogan, C., Ferry, A., Decostre, V., Hogrel, J.Y., Metzger, F., Hoeflich, A*., et al.* (2012). Molecular, physiological, and motor performance defects in DMSXL mice carrying >1,000 CTG repeats from the human DM1 locus. PLoS Genet *8*, e1003043.

Jeanson, L., Guerrera, I.C., Papon, J.F., Chhuon, C., Zadigue, P., Pruliere-Escabasse, V., Amselem, S., Escudier, E., Coste, A., and Edelman, A. (2014). Proteomic analysis of nasal epithelial cells from cystic fibrosis patients. PLoS One *9*, e108671.

Kaech, S., and Banker, G. (2006). Culturing hippocampal neurons. Nat Protoc *1*, 2406-2415.

Nishida, A., Iwata, H., Kudo, Y., Kobayashi, T., Matsuoka, Y., Kanai, Y., and Endou, H. (2004). Nicergoline enhances glutamate uptake via glutamate transporters in rat cortical synaptosomes. Biol Pharm Bull *27*, 817-820.

Peixoto, A., Monteiro, M., Rocha, B., and Veiga-Fernandes, H. (2004). Quantification of multiple gene expression in individual cells. Genome research *14*, 1938-1947.

Schindelin, J., Arganda-Carreras, I., Frise, E., Kaynig, V., Longair, M., Pietzsch, T., Preibisch, S., Rueden, C., Saalfeld, S., Schmid, B*., et al.* (2012). Fiji: an open-source platform for biological-image analysis. Nat Methods *9*, 676-682.

Schneider, C.A., Rasband, W.S., and Eliceiri, K.W. (2012). NIH Image to ImageJ: 25 years of image analysis. Nat Methods *9*, 671-675.

Servais, L., and Cheron, G. (2005). Purkinje cell rhythmicity and synchronicity during modulation of fast cerebellar oscillation. Neuroscience *134*, 1247-1259.

Seznec, H., Agbulut, O., Sergeant, N., Savouret, C., Ghestem, A., Tabti, N., Willer, J.C., Ourth, L., Duros, C., Brisson, E*., et al.* (2001). Mice transgenic for the human myotonic dystrophy region with expanded CTG repeats display muscular and brain abnormalities. Hum Mol Genet *10*, 2717-2726.

Seznec, H., Lia-Baldini, A.S., Duros, C., Fouquet, C., Lacroix, C., Hofmann-Radvanyi, H., Junien, C., and Gourdon, G. (2000). Transgenic mice carrying large human genomic sequences with expanded CTG repeat mimic closely the DM CTG repeat intergenerational and somatic instability. Hum Mol Genet *9*, 1185-1194.

Sugihara, I., and Furukawa, T. (1995). Potassium currents underlying the oscillatory response in hair cells of the goldfish sacculus. J Physiol *489 (Pt 2)*, 443-453.

Tanaka, K., Watase, K., Manabe, T., Yamada, K., Watanabe, M., Takahashi, K., Iwama, H., Nishikawa, T., Ichihara, N., Kikuchi, T*., et al.* (1997). Epilepsy and exacerbation of brain injury in mice lacking the glutamate transporter GLT-1. Science *276*, 1699-1702.